Double modulated differential THz-TDS for thin film dielectric characterization

Samuel P. Mickan[a,b,*], Kwang-Su Lee[b], Toh-Ming Lu[b], Jesper Munch[c], Derek Abbott[a], X.-C. Zhang[b,*]

[a]*Department of Electrical and Electronic Engineering, Centre for Biomedical Engineering (CBME), The University of Adelaide, Adelaide, SA 5005, Australia*
[b]*Department of Physics, Rensselaer Polytechnic Institute, Troy, NY 12180, USA*
[c]*Department of Physics, The University of Adelaide, Adelaide, SA 5005, Australia*

Abstract

Terahertz differential time-domain spectroscopy (DTDS) is a new technique that uses pulsed terahertz radiation to characterize the optical properties of thin dielectric films. Characterizing thin films in the GHz to THz range is critical for the development of new technologies in integrated circuitry, photonic systems and micro-electro-mechanical systems. There are potential applications for gene and protein chips. This paper shows how DTDS can be combined with double modulation in the pump-probe system to improve sensitivity by an order of magnitude. An iterative algorithm is presented to estimate the optical properties of a given thin film. The technique is experimentally verified using 1-μm-thick samples of silicon dioxide on silicon.
© 2002 Elsevier Science Ltd. All rights reserved.

Keywords: Terahertz; Thin films; Spectroscopy

1. Introduction

Thin film characterization is a fundamental application of optics and electronics. Terahertz time-domain spectroscopy (THz-TDS) is a technique developed in the last decade for characterizing samples in the THz band of the electro-magnetic spectrum. THz-TDS provides a new non-destructive method for probing thin films at speeds higher than network analyzers and wavelengths longer than optical sources. The high noise background associated with THz-TDS of very thin samples can be vastly improved by using terahertz differential time-domain spectroscopy (DTDS) and a scheme of double modulation.

Thin film characterization is important for the semi-conductor industry as it pushes for smaller and faster devices. Materials with an high dielectric constant are required for improved insulation, to stop tunnelling between layers, and low dielectric materials are needed for interconnects with reduced capacitance [1]. As feature sizes approach 100 nm and chip frequencies climb into the upper gigahertz range, it becomes increasingly important to have a convenient method of characterizing the THz properties of thin dielectric films [2]. Thin film dielectric materials are being explored for many applications. Interest in plastic-based electronics is spurring the development of organic–inorganic hybrid materials and organic transistors on plastic [3,4]. Single crystal optoelectronic devices are being developed for thin film transistors and MOEMS [5].

THz systems are non-contact, non-destructive and highly sensitive. Apart from applications in high speed device characterization, THz radiation has been used for sensitive quality control, chemical spectroscopy and biomedical diagnostics. THz penetrates optically opaque materials that cannot be characterized using optical methods, and can be used in transmission, reflection and tomographic experiments [6]. THz has the potential to become a widespread diagnostic tool in the future [7].

This paper firstly overviews the background of THz technology development, then looks at the problem of thin film characterization. A proposed solution to the thin film characterization problem is the DTDS scheme.

* Corresponding authors. Address: Department of Physics, Rensselaer Polytechnic Institute, Troy, NY 12180, USA. Tel.: +1-18-276-3096; fax: +1-518-276-6680.

E-mail addresses: spmickan@eleceng.adelaide.edu.au (S.P. Mickan), leek2@rpi.edu (K.S. Lee), lut@rpi.edu (T.-M. Lu), jmunch@physics. adelaide.edu.au (J. Munch), dabbott@eleceng.adelaide.edu.au (D. Abbott), zhangxc@rpi.edu (X.-C. Zhang).

The two primary innovations of this work are the incorporation of double modulation into the DTDS system and a more reliable method of material parameter estimation. We describe in some detail how the experiments were conducted and present results demonstrating the effectiveness of the DTDS technique. We conclude by discussing the future directions of our work and summarizing our results.

1.1. THz-TDS

THz (10^{12} Hz, $\lambda = 0.3$ mm) frequency radiation has historically been difficult to generate and detect [8]. Thermal sources have weak emission at long wavelengths and gas vapor lasers are cumbersome [9]. Bolometric detectors only operate under vacuum at liquid-helium temperatures [10]. Fourier transform infrared (FTIR) spectroscopy does offer spectroscopic information down to about 1 THz, but not into the GHz regime [11]. Research continues into many sources and detectors in the THz band, including germanium lasers, gas–vapor lasers, quantum cascade lasers and backward-wave oscillators [12–15].

The development of pulsed THz radiation (T-rays) generated using ultrafast optical lasers has provided a new method for accessing the THz frequency regime. Pulsed THz techniques were initially developed for waveguides and circuit characterization [16–18]. Free-space THz spectroscopy grew from the development of both photoconductive dipole antennas and electro-optic crystals as sources and detectors [19–22]. The spectroscopy of bulk dielectrics at THz frequencies was part of the early work in the field [23,24].

Recent developments in T-ray research are wide-reaching. T-rays have been extended to two-dimensional imaging using a variety of scanning and CCD techniques [25–29]. T-ray spatial resolution has been improved by the development of near field imaging [30–32]. T-ray systems now exhibit very high signal-to-noise ratios and are being implemented in applications including scaled 'radar' profiling and cancer detection [33–35].

2. Problem: THz-TDS of thin films

Thin film characterization is an important task for T-ray systems. Thin film analysis is limited by system sensitivity; the thickness of a thin film, being microns or less, is far less than the T-ray wavelength. A number of approaches have been used to increase system sensitivity, including DTDS, angle-depended spectroscopy, interferometry and planar waveguides.

There is a need for a THz frequency, non-contact, room temperature thin film characterization technique. Current methods of dielectric thin film characterization are summarized in Table 1, showing a gap in information from

Table 1
A comparison of methods for thin film characterization

Technique	Freq. range	Comments
Ellipsometry	20–800 THz	Optical technique [37]
FTIR	5–80 THz	For bulk and sheets [11]
Resonator	35–144 GHz	For sheets
Vector network analyzer	50 MHz to 100 GHz	Requires electrode patterning and complex analysis
RF impedance analyzer	1 MHz to 1 GHz	For circuits
LCR meter	10 Hz to 1 MHz	For circuits
C–V technique	DC and low freq.	Requires Hg probe contacts [38]

0.144 to 5 THz [36]. This is covered by the typical operating bandwidth of T-ray systems.

THz thin film characterization requires very high sensitivity. Even for a signal-to-noise ratio (SNR) of 10^7, it is difficult to see phase shifts that are less than the coherence length of the radiation [34]. Picosecond T-ray pulses with a bandwidth of approximately 2 THz and a center frequency of 0.8 THz have a coherence length of about 150 μm. The phase shift caused by a dielectric sample in the T-ray radiation path is proportional to $(\tilde{n} - 1)d/\lambda$, where $\tilde{n}$ is the complex refractive index of the medium, d is the sample thickness and λ is the T-ray wavelength. For small $\tilde{n}$ and d, this phase change is very difficult to detect in background noise.

The complex dielectric constant of a sample is related to its optical properties by the relation $\tilde{\epsilon} = (\tilde{n})^2$, where, for extinction coefficient κ and refractive index n, $\tilde{n} = n - j\kappa$. T-rays have been used to characterize a wide variety of materials using different techniques. T-rays can be used to observe static and dynamic characteristics of superconducting films, dielectrics in waveguides and DNA thin films [39–42]. Organic thin polymer films were first characterized by T-rays in 1992 [43]. A reliable algorithm for estimating the T-ray characteristics of thin film dielectrics was proposed in 1996 [44]. This method uses a model based on simple Fresnel equations and an iterative fit algorithm. The refractive index of a 10.2-μm-thick porous silicon layer was characterized with ±10% error, although estimation of the thin film extinction coefficient κ had ±100% error. Near-Brewster angle ('goniometric') phase shift reflection has been used to determine the refractive index of 3.27-μm-thick polymer films [36]. The Brewster-angle method uses a model based on Fresnel equations and an iterative fit to determine the refractive index. An incorporation of this technique into tomography has been suggested by angle-depended T-ray tomography of thin films for fuel cell applications [6].

Another method to increase the sensitivity of the T-ray system is interferometry. T-ray interferometric techniques typically induce a 180° (Gouy) phase shift in one arm of a Michelson interferometer, then detect phase changes introduced by a thin sample into one arm. Enhanced depth and spatial resolution have been

achieved with T-rays focused to a point on a reflective sample in one arm of an interferometer, where the Gouy shift occurs at the focal point on the sample [45]. The peak amplitude showed a 20% change for a 12.5-μm-thick air gap in Teflon. Another interferometer has been constructed using silicon prisms as reflectors, where the Gouy shift was induced by a fixed end reflection from one of the faces [46]. This study characterized the real and imaginary parts of the refractive index of a 2-μm-thick film of free-standing Mylar.

Using planar waveguides and a THz resonator, Bolivar et al. have demonstrated an highly sensitive device for probing the binding state of DNA [47]. This thin film microstripline approach can be extended to two-dimensional gene chips for high speed DNA analysis. The THz waveguide and resonator structure is sensitive to single-base defects in an 1.1 fmol volume of 0.52 g/l DNA-in-water. Although highly sensitive and integrable, this technique is not ideal for non-contact characterization of thin dielectric films.

The techniques described above have achieved spectroscopy and imaging of dielectrics of 1 μm thickness. The challenge remains, however, to extend T-ray frequency characterization to thinner films and lower dielectric constants. A promising technique for further improving T-ray system sensitivity is DTDS.

3. Proposed solution: differential THz-TDS

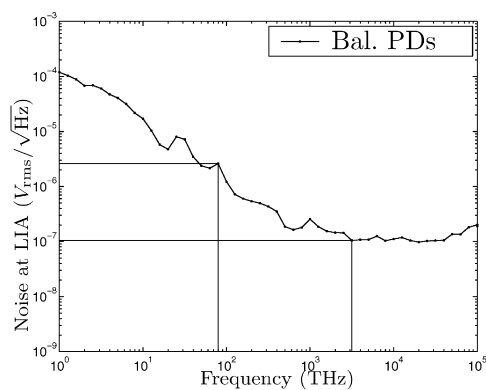The idea behind DTDS is to modulate the T-ray signal using only the thin film, and detect the magnitude of this modulation using a lock-in amplifier (LIA). The sample is a substrate half-covered with the film and half bare, as shown in Figs. 1 and 3(b).

DTDS is able to measure very subtle variations in phase and absorption. In a normal THz-TDS experiment, this difference is determined from the ratio of two spectra, S_{film}/S_{ref}, where the spectral components S are the Fourier Transforms of the time domain waveforms measured in the experiment. Each waveform is measured in a separate scan of the pump beam delay stage, so there is some time between the scans, up to 10 min or more for sensitive scans. For a typical T-ray system, the major source of noise is the pump laser, which is very sensitive to slow fluctuations in temperature and humidity. These fluctuations can cause larger changes in the detected T-ray signal than the thin film sample itself. The advantage of DTDS is that the signal transmitted through the film is compared to the signal through the substrate at each point of the delay stage. In effect, the differential waveform is equivalent to the difference between the reference and sample waveforms, $y_{diff} = y_{ref} - y_{film}$.

DTDS was first demonstrated in 2000 to determine the refractive index of an 1.8-μm-thick parylene-N film [52]. This first work developed an analytical expression for the refractive index of the film and dithered the sample at 16 Hz. An improvement on this work was to increase the dither frequency to 66 Hz, and thereby, reduce the noise in the detected T-rays [53]. Ultrafast lasers have an $1/f$ noise characteristic, so increasing the modulation frequency dramatically reduces noise [48–51]. To further increase the modulation frequency, we use double modulation.
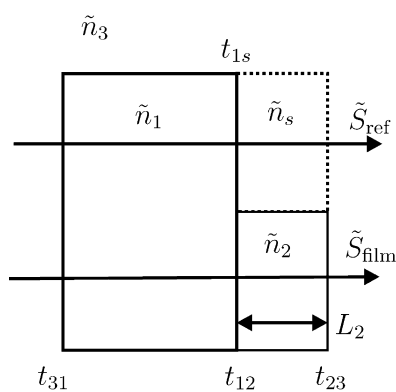
(a) Thin film schematic   (b) Noise spectrum of T-ray experiment

Fig. 1. (a) shows the schematic of a thin film sample prepared for DTDS. The thin film, characterized by the complex refractive index $\tilde{n}_2$, is supported by a substrate, $\tilde{n}_1$. The surrounding medium, in our case air, has the complex refractive index $\tilde{n}_3$. $\tilde{n}_s$ is the complex refractive index of the medium that replaces the volume of the thin film—in our experiments this is air, although if the thin layer is created by implantation of the substrate, $\tilde{n}_s$ may differ from $\tilde{n}_3$. The spectral components that are transmitted through the substrate are denoted by $\tilde{S}_{ref}$ and the components transmitted through the substrate and the film are denoted $\tilde{S}_{film}$. L_2 is the thickness of the thin film, measured using, for example, atomic force microscopy. The Fresnel transmission coefficients, t_{ab}, indicate the transmission from medium a to medium b, where $t_{ab} = 2\tilde{n}_a/(\tilde{n}_a + \tilde{n}_b)$. In DTDS, the signal is made up of the difference between $\tilde{S}_{ref}$ and $\tilde{S}_{film}$ by rapidly switching between them. (b) shows the noise spectrum of our T-ray system with balanced PDs. The noise spectrum shows an $1/f$ noise characteristic typical of ultrafast laser-driven experiments [48–51].The benefit of double modulation is highlighted by the two lines at 100 Hz and 3 kHz. The noise level at 3 kHz and above is more than an order of magnitude less than the noise at 100 Hz and below. The noise spectrum was measured using biased PDs, a 50-Ω load impedance and a LIA swept through different frequencies. The noise output of the LIA was measured with a settling time of 60 times the time constant.

3.1. Double modulation

Double modulation is a technique similar to encoding information on a carrier wave in telecommunications. The signal, already modulated at a lower frequency f_2, is additionally modulated at an higher frequency f_1 by an optical chopper. The frequency f_1, equivalent to the carrier frequency, is then removed in the detection system through demodulation. The advantage of double modulation is that the noise level at the higher modulation frequency is less than that at the lower frequency, as shown in Fig. 1(b).

The main source of noise in the DTDS experiment is the mode-locked Ti/sapphire laser, with an $1/f$ noise characteristic. Noise can be reduced by modulating the pump beam at some audio or radio frequency (RF) f_2 with a mechanical chopper, or an acousto- or electro-optic device. Once converted to an electronic signal with a photo detector of appropriate bandwidth, the depth of the modulation is detected with phase-sensitive detection, that is, a LIA. The LIA then passes the signal through a very narrow band filter to reject any variations not at the modulation frequency. Single frequency modulation is diagrammatically described in Fig. 2(a). The important quantity is the shaded area under the noise curve, which indicates the amount of noise appearing at the output of the LIA.

Ideally an experiment should be modulated at as high a frequency as possible. For mode-locked lasers, $1/f$ signal fluctuations dominate at frequencies below 3 MHz, where the shot noise limit is reached [55]. Unfortunately, it is impossible to shake the thin film sample above audio frequencies (AF) because of mechanical inertia. Galvanometric scanners do not have sufficient travel at frequencies above 100 Hz when a sample is attached. At modulation frequencies below 100 Hz, the $1/f$ noise levels are very high, greatly reducing the sensitivity of DTDS. Double modulation enables the use of a high carrier frequency, which sets the noise level, and an arbitrarily low shaker frequency. Galvanometer operation at a frequency less than 20 Hz, where $1/f$ noise is very high, eliminates heating problems and enables a larger shaking amplitude. The process of double modulation and demodulation is shown in Fig. 2(b).

To quantify the improvement in SNR due to double modulation, we have to consider both the decrease in noise level and the decrease in signal level it causes. Modulating the signal with a second modulator decreases its amplitude by half. Each modulator blocks 50% of the pump beam. If, however, the reduction in noise is better than 50%, then double modulation results in an improved SNR. In Fig. 1(b) we show the noise spectrum of our T-ray system, which uses balanced photodiode (PD) detection [56,57]. If the modulation frequency is set to 3 kHz or higher, the noise level drops by an order of magnitude compared to a modulation frequency of 100 Hz or lower. This is the improvement that we predict for a system dominated by $1/f$ noise.

A schematic layout of double modulation as implemented in our experiment is shown in Fig. 3(a). The pump beam is first modulated at f_1 by the mechanical
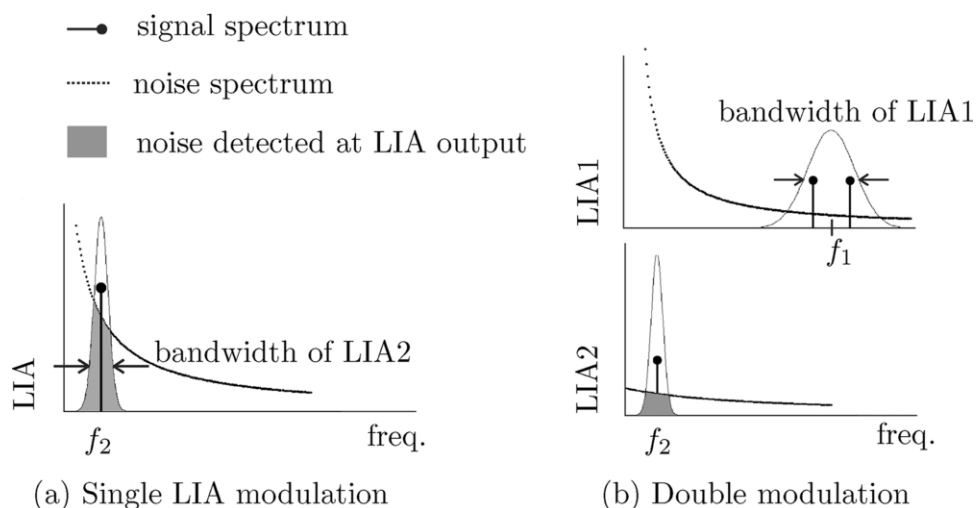

Fig. 2. This figure is a diagrammatic comparison of single and double modulation. (a) shows an experiment with a single LIA. The signal is modulated at a frequency f_2 by, in our case, a galvanometric shaker. Although the signal is chopped by a square wave, the LIA detects the fundamental sine wave, so we consider it to be a single frequency spike. The LIA has a certain bandwidth, set by its time constant, and the noise at the LIA output is determined by the noise power within that bandwidth, which corresponds to the shaded region. (b) demonstrates the operation of double modulation. In double modulation, the signal at the input to the first LIA is found at the sum and difference of the modulation frequencies, $f_1 + f_2$ and $f_1 - f_2$. The first LIA acts as a frequency mixer and demodulates the f_1 frequency, so that at the input of the second LIA, the signal is modulated at f_2. The advantage of DTDS is that the noise found at the output of the second LIA is far less than in the single LIA set-up. One important point is that the bandwidth of the first LIA has to be set sufficiently wide to allow the signal to pass through at a frequency $\pm f_2$ from the center frequency. Double modulation can be achieved using a LIA driven by a synthesized frequency $f_1 + f_2$, unless the sum frequency is at RF. In that case, it is advantageous to have the second LIA operating at AF because an AF LIA has better operating characteristics than an RF LIA [54].
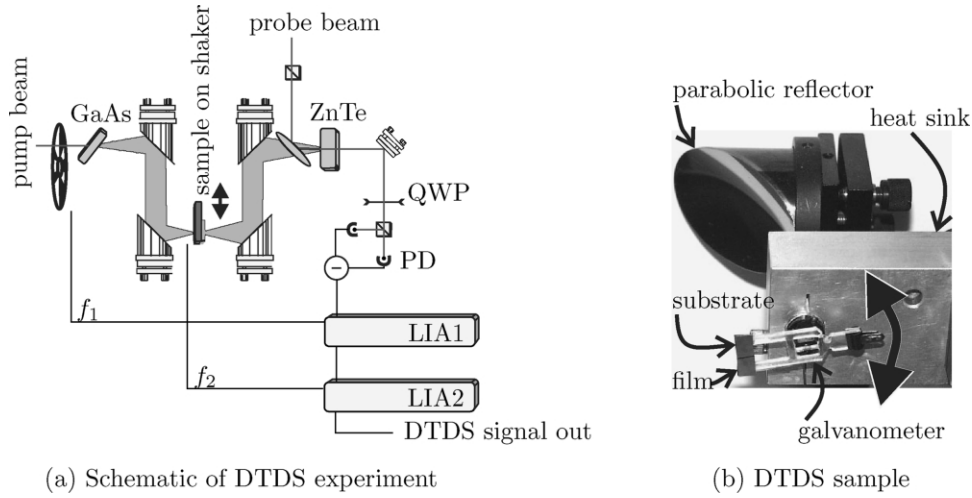
Fig. 3. DTDS experimental set-up. (a) shows a schematic of the DTDS experiment. The pump and probe beams are split from the ultrafast laser. (b) shows a photograph of the DTDS thin film sample held by the galvanometric scanning arm. In the background of the photograph is a paraboloidal reflector for collimating the T-rays between sample and detector. The large arrow indicates the galvanometer's motion. This experimental set-up is explained in Section 4.

chopper and then modulated at f_2 by the dithered thin film sample. The double modulated T-ray signal is converted to a polarization modulation of the probe beam using electro-optic detection [22]. Balanced PDs detect the polarization modulation of the probe beam, and the first LIA, acting as a mixer, demodulates the chopper f_1. The second LIA detects the thin film signal at f_2 and provides a complex output representing the DTDS waveform at a given pump-probe delay.

3.2. Parameter estimation

Material parameters in THz-TDS must be estimated from the time-domain data using methods similar to Fourier transform spectroscopy [60]. In essence, a pulse that has been transmitted through or reflected from the sample contains absorption and phase delay information about the sample. The effect on the pulse caused only by the sample is determined by deconvolving the sample pulse with a reference pulse [61]. The deconvolved signal is compared to a model based on Fresnel equations to determine its frequency-dependent complex refractive index, $\tilde{n}(\omega) = n(\omega) - j\kappa(\omega)$, where n and κ are the refractive index and extinction coefficient of the sample material, respectively, [62].

Eq. (1) models the complex transmission spectrum of normal THz-TDS.

$$T_{\text{model}} = \frac{2\tilde{n}_2(\tilde{n}_1+\tilde{n}_3)}{(\tilde{n}_2+\tilde{n}_1)(\tilde{n}_2+\tilde{n}_3)}\exp\left[-i(\tilde{n}_2-\tilde{n}_s)\frac{\omega L}{c_0}\right]\text{FP}(\omega), \quad (1)$$

where the complex refractive indices $\tilde{n}_*$ and the film thickness L are defined in Fig. 1(a), ω and c_0 are the angular frequency and speed of light in a vacuum, and $\text{FP}(\omega)$ is the frequency dependent contribution of Fabry–Pérot reflections in the thin film [44].

The complex refractive index of the sample can be estimated using this model either by iterative approximation or, in some situations, analytically. If the sample is sufficiently thick so no Fabry–Pérot reflections are present, or if the successive reflections can be isolated from each other, then analytic expressions for n and κ can be found with some approximation [63] For thin film samples, however, Fabry–Pérot reflections overlap in the primary T-ray pulse. To estimate parameters in our experiment, we
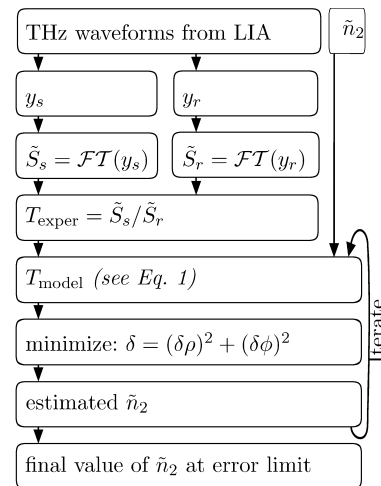

Fig. 4. The reliable parameter estimation algorithm proposed by Duvillaret et al. [44]. The time-domain THz waveforms y_s and y_r are obtained experimentally. An estimate of $\tilde{n}_2$ is provided as seed for the search algorithm, which operates to minimize the error metric δ, where $\delta\rho = \log|T_{\text{model}}| - \log|T_{\text{exper}}|$, and $\delta\phi = \arg(T_{\text{model}}) - \arg(T_{\text{exper}})$. The re-estimation step is performed with Matlab's fminsearch function, which minimizes a function of several variables, using the simplex search algorithm of Lagarias et al. [58,59]. This algorithm takes approximately 0.6 s to estimate the complex refractive index $\tilde{n}_2$ for each frequency of interest, given 1024 data points in the FFTs and an 1.5-GHz Pentium 4 processor.
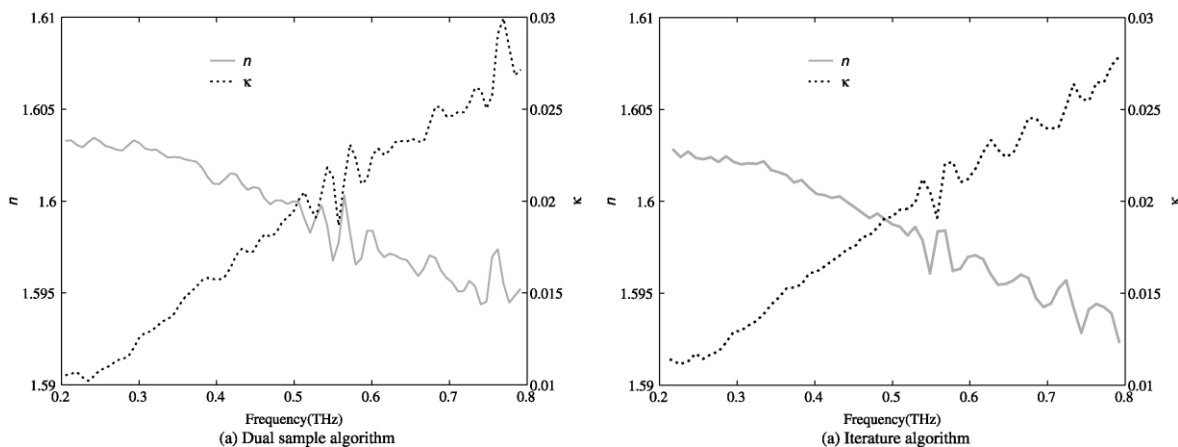
Fig. 5. Test of the iterative parameter estimation algorithm shown in Fig. 4. The parameters in (a) were estimated using dual sample spectroscopy. In dual sample spectroscopy, two samples of the same material are used. The samples have different thicknesses, both sufficiently large to avoid Fabry–Pérot reflections. In this case, the two samples were polyethylene blocks of thicknesses 11.4 and 4.73 mm. The T-ray waveform transmitted through the thin sample is used as the reference, so all Fresnel transmission coefficients at the interfaces are automatically accounted for. The advantage of dual sample spectroscopy is that simple and exact analytical expressions to estimate $\tilde{n}_2$ can be easily derived. The parameters in (b) were estimated using the iterative approximation algorithm. The correspondence between the results in (a) and (b) confirms the accuracy of the iterative algorithm.

used an iterative approximation technique represented by the flow chart in Fig. 4. We substituted the difference between the reference and differential waveforms for the sample waveform in the equations, that is $S_s \equiv S_r - S_d$. The advantage of using this substitution rather than separately deriving the model equation T_{model} for DTDS is that we can confirm the accuracy of our algorithm with standard THz-TDS data.

To confirm that the data processing algorithm was correct, we performed two tests. Firstly, we used the standard DTDS algorithm to characterize a simple test subject, and secondly, we confirmed that our model matched the experiment once the complex refractive index had been estimated. Fig. 5(b) shows the refractive index of a test sample calculated using two different-thickness samples. The test sample is bulk polyethylene. Fig. 5(b) shows the refractive index of one of the polyethylene samples calculated using the iterative algorithm depicted in Fig. 4. This test confirmed that our parameter estimation algorithm was correct.

To confirm that our model gives transmission data matching the experimental data for the estimated values of $\tilde{n}_2$, we plotted the experimental transmission spectrum and the modelled transmission spectrum in Fig. 6. The line

(a) Magnitude of transmission spectrum
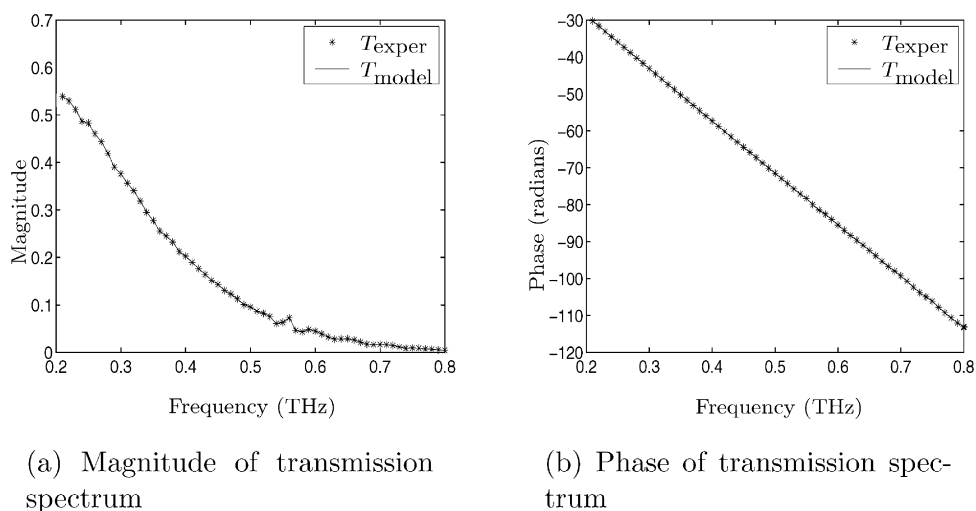
(b) Phase of transmission spectrum

Fig. 6. Plot of modelled and experimental transmission spectra. These plots confirm that our estimated refractive index and extinction coefficient values do correctly model the transmission spectrum of the experiment. These data are from an 11.4-mm-thick block of polyethylene plastic and the algorithm depicted in Fig. 4.
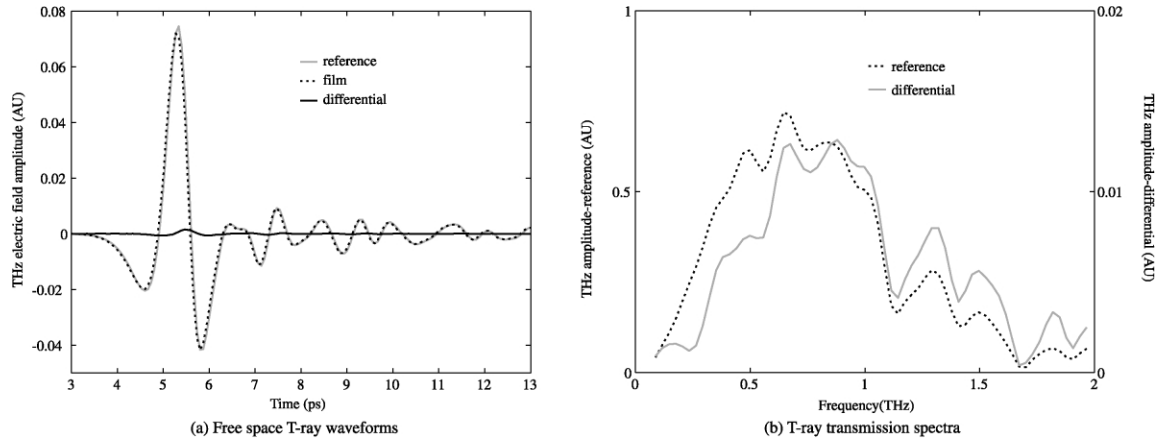
Fig. 7. Experimental T-ray time-domain waveforms and spectra. (a) shows the reference waveform through the substrate, the waveform through the film, and the differential signal. This figure shows only the real part of the signal, corresponding to the X channel of the LIA. The Y channel waveform is an order of magnitude smaller. The substrate is a 0.5-mm-thick wafer of high-resistivity silicon, refractive index 3.44. The film is a 0.935-μm-thick layer of silicon dioxide deposited on the silicon. The film was prepared by thermal oxidation on the (100) surface of a p-type silicon wafer at 800–1000 °C. These measurements were taken with an LIA time constant of 300 ms, at room temperature. (b) shows the transmission spectra of the reference and differential T-ray waveforms. Phase information is linear and is not shown in these plots. The bandwidth of the reference pulse is typical for our T-ray system, driven as it is by T-ray generation from a GaAs surface using 100-fs optical pulses. The absorption lines at 0.56, 0.75, 1.1–1.2 and 1.4 THz are caused by water vapor in the air [67].

from the modelled transmission spectrum T_{model} and the stars from the experimental data T_{exper} show a one-to-one correspondence.

4. Experimental set-up

Our T-ray system is a typical system, using a semi-conductor T-ray source and electro-optic detection [64–66].

The optical layout is shown in Fig. 3(a). Our ultrafast laser is a Spectra-Physics Tsunami Ti/sapphire oscillator, multi-line pumped by a Spectra-Physics BeamLoc large frame argon-ion laser, and producing 1.7 W average power of 100-fs pulses at an 82-MHz repetition rate.[1] Our pump beam power is about 800 mW after passing through a mechanical chopping wheel, which modulates the beam at f_1. T-rays are generated by ultrafast current transients in a thin GaAs wafer mounted at Brewster's angle to the beam. The T-rays are collimated and focused with off-axis gold-coated paraboloidal reflectors, and detected in a collinear geometry in a 2-mm-thick $\langle 110 \rangle$-oriented ZnTe crystal. The probe beam power is approximately 100 mW and we detect 1 mA of current in each of the balanced PDs. The polarization rotation of the probe beam is detected by a Wollaston analyzer and balanced PDs. A quarter wave plate (QWP) is used to compensate for the intrinsic birefringence in the ZnTe. The difference current from the PDs, proportional to the T-ray electric field, is filtered by two LIAs, as described in Section 3.1.

The sample is held in a galvanometric shaker from Cambridge Technology[2] cambridgetech, operating at f_2,

shown in Fig. 3(b). The shaker is mounted in a large aluminium heat sink to keep its operating temperature below 50°C. The heat sink, despite its proximity to the T-ray beam path, has less than 1% effect on the transmitted T-ray waveforms. The SiO_2 film can be seen covering half the Si substrate. On the reverse of the sample is a small aluminum square, used as a chopper to take the reference waveform. The diameter of the T-ray spot on the sample is less than 1 mm.

Various thin films have been characterized in this system, including 0.934-μm-thick SiO_2 on silicon. The SiO_2 thin films in our experiment were prepared by HF etching half of the SiO_2 deposited on the Si wafer. The samples were characterized under normal indoor conditions, with approximately 25 °C and 35% humidity. The parameter estimation was performed as described in Section 3.2.

5. Results

The results of this experiment demonstrate the accuracy of the DTDS technique for extracting the refractive index and extinction coefficient of a thin film.

The raw time domain data from a DTDS experiment are shown in Fig. 7(a). For a 1-μm-thick film, the difference between the waveforms propagated through the substrate and through the film is almost indistinguishable. The differential signal is far smaller than the other waveforms, and is 90° out of phase with the reference waveform. The DTDS technique was first called *differential* because the DTDS signal is an approximate differentiation of the reference signal with respect to time; the optical delay caused by moving the thin film into the beam path is a very small Δt. By measuring the small change in amplitude of
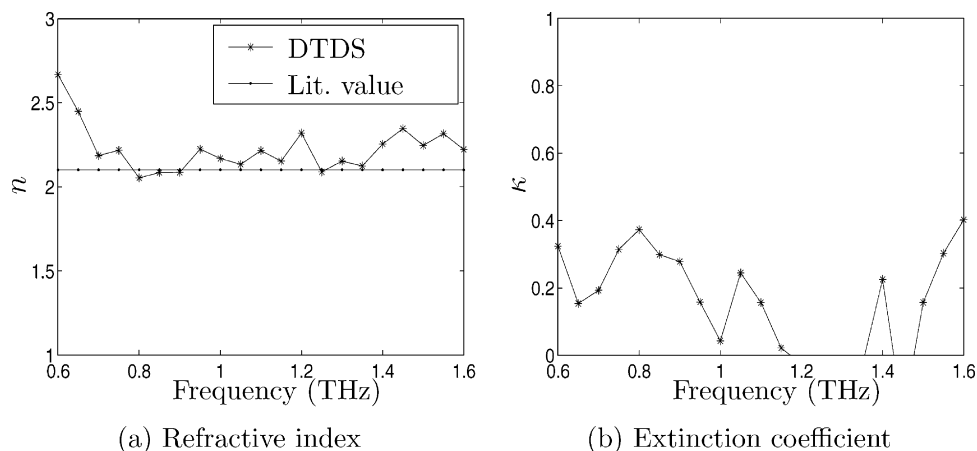
(a) Refractive index (b) Extinction coefficient

Fig. 8. Estimated optical parameters of SiO_2 thin film. The refractive index n is comparable to values for SiO_2 given in the literature ($n = 2.1$) [68]. The literature value for the extinction coefficient has been omitted because there is some disagreement on its value at this frequency. The bandwidth of these measurements is limited primarily by the limited bandwidth of the differential signal, whose spectrum is shown in Fig. 7(b). The error in the estimates of n and κ is about ± 0.2.

the transmitted signal, Δy, and plotting as a function of time delay, one is approximately measuring the slope of the reference waveform, dy/dt.

The amplitude spectra of the reference and differential waveforms are plotted in Fig. 7(b). The 0.2–2 THz bandwidth of the reference pulse is typical for this 100-fs laser T-ray system. The strong absorption lines are due to water vapor in the air [67]. The water lines are a multiplicative effect on the THz spectra, thus they are removed in the deconvolution process. The problem they represent is a lower SNR at those frequencies. The differential signal has a reduced bandwidth because the amplitude is more submerged in the noise, although the approximate shape is the same as the reference spectrum.

Fig. 8 shows the estimated optical parameters of an SiO_2 thin film from 600 GHz to 1.6 THz. The experimental values, indicated by crosses, are compared to the predicted values in the literature [68]. Although there is some variation in the estimated parameters due to noise, they correspond to the predicted value of refractive index and extinction coefficient within ± 0.2. The error in refractive index is $\pm 10\%$ and in the extinction coefficient $\pm 100\%$. These results confirm that our technique can be used to estimate the optical parameters of thin films with reasonable accuracy.

6. Future directions and conclusions

There are a number of system improvements and potential applications that remain to be explored in DTDS. We expect that the noise of the system can be further reduced by using a modulation frequency higher than 3 kHz, coupled with an RF LIA. We are also considering a technique of dual thickness DTDS, where the difference signal between two thicknesses of the same material is measured. Such a technique would enable us to have a far simpler parameter estimation algorithm.

We will be applying the DTDS method to characterize thin biomolecular films for lab-on-a-chip applications. It will be valuable to be able to non-invasively probe the hydration, conformation and activity of protein films used, for example, as enzyme catalysts layered on inorganic substrates. DTDS is an ideal tool for such research.

We have demonstrated the application of double modulation to improve the SNR of DTDS by an order of magnitude, and we have developed and tested an algorithm to enable reliable optical parameter extraction from thin films.

Acknowledgements

References

[1] M.L. Green, E.P. Gusev, R. Degraeve, E.L. Garfunkel, Ultrathin (<4 nm) SiO_2 and Si–O–N gate dielectric layers for silicon microelectronics: understanding the processing, structure, and physical and electrical limits, Journal of Applied Physics 90 (5) (2001) 2057–2121.

[2] A.I. Kingon, J.-P. Maria, S.K. Streiffer, Alternative dielectrics to silicon dioxide for memory and logic devices, Nature 406 (6779) (2000) 1032–1038.

[3] C.R. Kagan, D.B. Mitzi, C.D. Dimitrakopoulos, Organic-inorganic hybrid materials as semiconducting channels in thin-film field-effect transistors, Science 286 (5441) (1999) 945–947.

[4] C.D. Dimitrakopoulos, S. Purushothaman, J. Kymissis, A. Callegari, J. Shaw, Low-voltage organic transistors on plastic comprising high-dielectric constant gate insulators, Science 283 (5403) (1999) 822–824.

[5] F.-J. Meyer zu Heringdorf, M.C. Reuter, R.M. Tromp, Growth dynamics of pentacene thin films, Nature 412 (6846) (2001) 517–520.

[6] M. Brucherseifer, P. Haring Bolívar, H. Klingenberg, H. Kurz, Angle-dependent THz tomography—characterization of thin ceramic oxide films for fuel cell applications, Applied Physics B: Lasers and Optics 72 (3) (2001) 361–366.

[7] T. Clancy, S.R. Pieczenik, Op-Center: Games of State, Mass Market Paperback, 1996.

[8] M.C. Nuss, J. Orenstein, Terahertz time-domain spectroscopy, in: G. Grüner (Ed.), Millimeter and submillimeter wave spectroscopy of solids, Topics in Applied Physics, vol. 74, Springer, Berlin, Germany, 1998, pp. 7–50, Chapter 2.

[9] B. Lax, Applications of far infrared lasers, in: A. Mooradian, T. Jaeger, P. Stokseth (Eds.), Tunable Lasers and Applications, Springer Series in Optical Sciences, vol. 3, Springer, Berlin, 1976, pp. 340–347.

[10] S.P. Mickan, D. Abbott, J. Munch, X.-C. Zhang, T. van Doorn, Analysis of system trade-offs for terahertz imaging, Microelectronics Journal 31 (7) (2000) 503–514.

[11] P.Y. Han, M. Tani, M. Usami, S. Kono, R. Kersting, X.-C. Zhang, A direct comparison between terahertz time-domain spectroscopy and far-infrared Fourier transform spectroscopy, Journal of Applied Physics 89 (4) (2001) 2357–2359.

[12] E. Bründermann, D.R. Chamberlin, E.E. Haller, Novel design concepts of widely tunable germanium terahertz lasers, Infrared Physics and Technology 40 (3) (1999) 141–151.

[13] M. Jackson, E.M. Telles, M.D. Allen, K.M. Evenson, Short-wavelength far-infrared laser cavity yielding new laser emissions in CD$_3$OH, Applied Physics B: Lasers and Optics 72 (7) (2001) 815–818.

[14] S.S. Dhillon, A.G. Davies, R. Harrell, E.H. Linfield, D.A. Ritchie, M. Pepper, D.D. Arnone, Terahertz (THz) electro-luminescence from AlGaAs–GaAs quantum cascade heterostructures, Conference on Lasers and Electro-Optics '01, Optical Society of America, Baltimore, MD, USA, 2001, pp. 483–484.

[15] A. Pimenov, A.V. Pronin, A. Loidl, A.P. Kampf, S.I. Krasnosvo-bodtsev, V.S. Nozdrin, Submillimeter spectroscopy of tilted Nd$_{1.85-}$Ce$_{0.15}$CuO$_{4-\delta}$ films: Observation of a mixed ac-plane excitation, Applied Physics Letters 77 (3) (2000) 429–431.

[16] D.H. Auston, M.C. Nuss, Electrooptic generation and detection of femtosecond electrical transients, IEEE Journal of Quantum Electronics 24 (2) (1988) 184–197.

[17] J.A. Valdmanis, G.A. Mourou, C.W. Gabel, Subpicosecond electrical sampling, IEEE Journal of Quantum Electronics 19 (4) (1983) 664–667.

[18] M.Y. Frankel, J.F. Whitaker, G.A. Mourou, Optoelectronic transient characterization of ultrafast devices, IEEE Journal of Quantum Electronics 28 (10) (1992) 2313–2324.

[19] D.H. Auston, K.P. Cheung, Coherent time-domain far-infrared spectroscopy, Journal of the Optical Society of America B: Optical Physics 2 (4) (1985) 606–612.

[20] C. Fattinger, D. Grischkowsky, Point source terahertz optics, Applied Physics Letters 53 (16) (1988) 1480–1482.

[21] B.B. Hu, X.-C. Zhang, D.H. Auston, Free-space radiation from electro-optic crystals, Applied Physics Letters 56 (6) (1990) 506–508.

[22] Q. Wu, X.-C. Zhang, Free-space electro-optic sampling of terahertz beams, Applied Physics Letters 67 (24) (1995) 3523–3525.

[23] Y. Pastol, G. Arjavalingham, J.-M. Halbout, G.V. Kopscay, Coherent broadband microwave spectroscopy using picosecond optoelectronic antennas, Applied Physics Letters 54 (4) (1989) 307–309.

[24] D. Grischkowsky, S. Keiding, M. van Exter, C. Fattinger, Far-infrared time-domain spectroscopy with terahertz beams of dielectrics and semiconductors, Journal of the Optical Society of America B: Optical Physics 7 (10) (1990) 2006–2015.

[25] B.B. Hu, M.C. Nuss, Imaging with terahertz waves, Optics Letters 20 (16) (1995) 1716–1718.

[26] D.M. Mittleman, M. Gupta, R. Neelamani, R.G. Baraniuk, J.V. Rudd, M. Koch, Recent advances in terahertz imaging, Applied Physics B: Lasers and Optics 68 (6) (1999) 1085–1094.

[27] Z. Jiang, X.G. Xu, X.-C. Zhang, Improvement of terahertz imaging with a dynamic subtraction technique, Applied Optics 39 (17) (2000) 2982–2987.

[28] Q. Chen, M. Tani, Z. Jiang, X.-C. Zhang, Electro-optic transceivers for terahertz-wave applications, Journal of the Optical Society of America B: Optical Physics 18 (6) (2001) 823–831.

[29] A.B. Ruffin, J. Decker, L. Sanchez-Palencia, L. Le Hors, J.F. Whitaker, T.B. Norris, J.V. Rudd, Time reversal and object reconstruction with single-cycle pulses, Optics Letters 26 (10) (2001) 681–683.

[30] Q. Chen, Z. Jiang, G.X. Xu, X.-C. Zhang, Near-field terahertz imaging with a dynamic aperture, Optics Letters 25 (15) (2000) 1122–1124.

[31] O. Mitrofanov, I. Brener, M.C. Wanke, R.R. Ruel, J.D. Wynn, A.J. Bruce, J. Federici, Near-field microscope probe for far infrared time domain measurements, Applied Physics Letters 77 (4) (2000) 591–593.

[32] O. Mitrofanov, I. Brener, R. Harel, J.D. Wynn, L.N. Pfeiffer, K.W. West, J. Federici, Terahertz near-field microscopy based on a collection mode detector, Applied Physics Letters 77 (22) (2000) 3496–3498.

[33] R.A. Cheville, D. Grischkowsky, Time domain terahertz impulse ranging studies, Applied Physics Letters 67 (14) (1995) 1960–1962.

[34] Z.G. Lu, P. Campbell, X.-C. Zhang, Free-space electro-optic sampling with a high-repetition-rate regenerative amplified laser, Applied Physics Letters 71 (5) (1997) 593–595.

[35] R.M. Woodward, B. Cole, V.P. Wallace, D.D. Arnone, R. Pye, E.H. Linfield, M. Pepper, A.G. Davies, Terahertz pulse imaging of in-vitro basal cell carcinoma samples, Conference on Lasers and Electro-Optics '01, Optical Society of America, Baltimore, MD, USA, 2001, pp. 329–330.

[36] M. Li, G.C. Cho, T.-M. Lu, X.-C. Zhang, S.-Q. Wang, J.T. Kennedy, Time-domain dielectric constant measurement of thin film in GHz–THz frequency range near Brewster angle, Applied Physics Letters 74 (15) (1999) 2113–2115.

[37] A. Ulman (Eds.), Materials Characterization, Butterworth/Heinemann, Stoneham, MA, 1995.

[38] D.K. Schroder, Semiconductor Material and Device Characterization, Wiley, New York, 1990.

[39] M. Tonouchi, M. Yamashita, M. Hangyo, Vortex penetration in YBCO thin film strips observed by THz radiation imaging, Physica B 284–288 (2000) 853–854.

[40] D.R. Grischkowsky, Optoelectronic characterization of transmission lines and waveguides by terahertz time-domain spectroscopy, IEEE Journal of Selected Topics in Quantum Electronics 6 (6) (2000) 1122–1135.

[41] G. Gallot, S.P. Jamison, R.W. McGowan, D. Grischkowsky, Terahertz waveguides, Journal of the Optical Society of America B: Optical Physics 17 (5) (2000) 851–863.

[42] M. Brucherseifer, M. Nagel, P. Haring Bolívar, H. Kurz, A. Bosserhoff, R. Büttner, Label-free probing of the binding state of DNA by time-domain terahertz sensing, Applied Physics Letters 77 (24) (2000) 4049–4051.

[43] M. Ree, K.-J. Chen, D.P. Kirby, N. Katzenellenbogen, D. Grischkowsky, Anisotropic properties of high-temperature polyimide thin films: dielectric and thermal-expansion behaviors, Journal of Applied Physics 72 (5) (1992) 2014–2021.

[44] L. Duvillaret, F. Garet, J.-L. Coutaz, A reliable method for extraction of material parameters in terahertz time-domain spectroscopy, IEEE Journal of Selected Topics in Quantum Electronics 2 (3) (1996) 739–746.

[45] J.L. Johnson, T.D. Dorney, D.M. Mittleman, Enhanced depth resolution in terahertz imaging using phase-shift interferometry, Applied Physics Letters 78 (6) (2001) 835–837.

[46] S. Krishnamurthy, M.T. Reiten, S.A. Harmon, R.A. Cheville, Characterization of thin polymer films using terahertz time-domain interferometry, Applied Physics Letters 79 (6) (2001) 875–877.

[47] M. Nagel, P. Haring Bolívar, M. Brucherseifer, H. Kurz, A. Bosserhoff, R. Büttner, Integrated THz technology for label-free genetic diagnostics, Applied Physics Letters 80 (1) (2002) 154–156.

[48] D. von der Linde, Characterization of the noise in continuously operating mode-locked lasers, Applied Physics B: Photophysics and Laser Chemistry 39 (4) (1986) 201–217.

[49] H.A. Haus, A. Mecozzi, Noise of mode-locked lasers, IEEE Journal of Quantum Electronics 29 (3) (1993) 983–996.

[50] J. Son, J.V. Rudd, J.F. Whitaker, Noise characterization of a self-mode-locked Ti:sapphire laser, Optics Letters 17 (10) (1992) 733–735.

[51] A. Poppe, L. Xu, F. Krausz, C. Spielmann, Noise characterization of sub-10-fs Ti:sapphire oscillators, IEEE Journal of Selected Topics in Quantum Electronics 4 (2) (1998) 179–184.

[52] Z. Jiang, M. Li, X.-C. Zhang, Dielectric constant measurement of thin films by differential time-domain spectroscopy, Applied Physics Letters 76 (22) (2000) 3221–3223.

[53] K.-S. Lee, J.Y. Kim, J. Fortin, Z. Jiang, M. Li, T.-M. Lu, X.-C. Zhang, Dielectric property measurement of sub-micron thin films by differential time-domain spectroscopy, in: T. Elsaesser, S. Mukamel, M.M. Murnane, N.F. Scherer (Eds.), Ultrafast Phenomena XII, Springer Series in Chemical Physics, vol. 66, Springer, Berlin, 2000, pp. 232–234.

[54] S.V. Frolov, Z.V. Vardeny, Double-modulation electro-optic sampling for pump-and-probe ultrafast correlation measurements, Review of Scientific Instruments 69 (3) (1998) 1257–1260.

[55] L. Andor, A. Lörincz, J. Siemion, D.D. Smith, S.A. Rice, Shot-noise-limited detection scheme for two-beam laser spectroscopies, Review of Scientific Instruments 55 (1) (1984) 64–67.

[56] B.R. Hemenway, H.K. Heinrich, J.H. Goll, Z. Xu, D.M. Bloom, Optical detection of charge modulation in silicon integrated circuits using a multimode laser-diode probe, IEEE Electron Device Letters 8 (8) (1987) 344–346.

[57] J.M. Zhang, R.L. Ruo, M.K. Jackson, Noise suppression in Ti:sapphire laser-based electro-optic sampling, Applied Physics Letters 75 (22) (1999) 3446–3448.

[58] MATLAB, The MathWorks, Inc., `fminsearch`, http://www.mathworks.com/access/helpdesk/help/techdoc/ref/fminsearch.shtml.

[59] J.C. Lagarias, J.A. Reeds, M.H. Wright, P.E. Wright, Convergence properties of the Nelder–Mead simplex method in low dimensions, SIAM Journal of Optimization 9 (1) (1998) 112–147.

[60] A.G. Marshall, F.R. Verdun, Fourier Transforms in NMR, Optical, and Mass Spectroscopy, Elsevier, Amsterdam, The Netherlands, 1990.

[61] B. Ferguson, D. Abbott, Signal processing for T-ray bio-sensor systems, Proceedings of SPIE's Symposium on Smart Materials and MEMS, vol. 4236, SPIE, Melbourne, Australia, 2000, pp. 157–169.

[62] M. Born, E. Wolf, Principles of Optics, sixth edition., Cambridge University Press, Cambridge, 1997.

[63] L. Duvillaret, F. Garet, J.-L. Coutaz, Noise analysis in THz time-domain spectroscopy and accuracy enhancement of optical constant determination, Proceedings of SPIE—Terahertz Spectroscopy and Applications, vol. 3617, 1999, pp. 38–48.

[64] Z. Jiang, X.-C. Zhang, Terahertz imaging via electrooptic effect, IEEE Transactions on Microwave Theory and Techniques 47 (12) (1999) 2644–2650.

[65] X.-C. Zhang, B.B. Hu, J.T. Darrow, D.H. Auston, Generation of femtosecond electromagnetic pulses from semiconductor surfaces, Applied Physics Letters 56 (11) (1990) 1011–1013.

[66] M. Li, F.G. Sun, G.A. Wagoner, M. Alexander, X.-C. Zhang, Measurement and analysis of terahertz radiation from bulk semiconductors, Applied Physics Letters 67 (1) (1995) 25–27.

[67] M. van Exter, C. Fattinger, D. Grischkowsky, Terahertz time-domain spectroscopy of water vapor, Optics Letters 14 (20) (1989) 1128–1130.

[68] E.D. Palik, Handbook of Optical Constants of Solids, Academic Press, New York, 1985.